2022-09-29

Unraveling the formation region and frequency of chorus spectral gaps

Unraveling the formation region and frequency of chorus spectral gaps

Jinxing Li[1*] (http://orcid.org/0000-0003-0500-1056)
Jacob Bortnik[1] (https://orcid.org/0000-0001-8811-8836)
Wen Li[2] (https://orcid.org/0000-0003-3495-4550)
Xin An[3] (http://orcid.org/0000-0003-2507-8632)
Larry R. Lyons[1] (https://orcid.org/0000-0002-9867-3638)
William S. Kurth[4] (http://orcid.org/0000-0002-5471-6202)
George B. Hospodarsky[4] (http://orcid.org/0000-0001-9200-9878)
David P. Hartley[4] (https://orcid.org/0000-0001-8630-8054)
Geoffrey D. Reeves[5,6] (https://orcid.org/0000-0002-7985-8098)
Herbert O. Funsten[7] (https://orcid.org/0000-0002-6817-1039)
J. Bernard Blake[8] (https://orcid.org/0000-0001-7439-4362)
Harlan Spence[9] (https://orcid.org/0000-0002-2526-2205)
Daniel N. Baker[10] (https://orcid.org/0000-0001-5909-0926)

[1]Department of Atmospheric and Oceanic Sciences, University of California, Los Angeles, California, 90095, USA

[2]Center for Space Physics, Boston University, Boston, Massachusetts, 02215, USA

[3]Department of Atmospheric and Oceanic Sciences and Department of Earth, Planetary, and Space Sciences, University of California, Los Angeles, Los Angeles, California, 90095, USA

[4]Department of Physics and Astronomy, University of Iowa, Iowa City, Iowa, 52242-1479, USA

[5]Space Science and Applications Group, Los Alamos National Laboratory, Los Alamos, New Mexico, 87544, USA

[6]Los Alamos National Laboratory, MS-D466, PO Box 1663, Los Alamos, New Mexico, 87545, USA

[7]The New Mexico Consortium, Los Alamos, New Mexico, 87544, USA

[8]Space Science Applications Laboratory, The Aerospace Corporation, El Segundo, California, 90245, USA

[9]Institute for the Study of Earth, Oceans, and Space, University of New Hampshire, Durham, New Hampshire 03824-3525, USA

[10]Laboratory for Atmospheric and Space Physics, University of Colorado, Boulder, Colorado 80303-7814, USA

*Corresponding Author: Jinxing Li (jinxing.li.87@gmail.com)

Key Points

1) Chorus spectral gaps are formed near the equatorial source region where parallel and anti-parallel emissions are interleaved

2) Landau resonance causes electron parallel acceleration and phase space density isotropization around half electron Alfven velocity, which increases with latitudes

3) Chorus spectral gaps are usually found below 0.5 f_{ce} due to electron anisotropy reduction caused by Landau resonance at high latitudes

Abstract

The present study addresses two basic questions related to banded chorus waves in the Earth's magnetosphere: 1) are chorus spectral gaps formed near the equatorial source region or during propagation away from the equator? and 2) why are chorus spectral gaps usually located below 0.5 f_{ce} (f_{ce}: electron gyro-frequency)? By analyzing Van Allen Probes data, we demonstrate that chorus spectral gaps are observed in the source region where chorus waves propagate both in the parallel and anti-parallel directions to the magnetic field. Chorus spectral gaps below 0.5 f_{ce} are associated with electron parallel acceleration at energies above the equatorial Landau resonant energies. We explain that initially generated chorus waves quickly isotropize the electron distribution through Landau resonant acceleration, and the isotropization occurs for higher energies at higher latitudes. The isotropized population, after returning to the magnetic equator, leads to a chorus gap typically below 0.5 f_{ce} by suppressing wave excitation.

Plain Language Abstract

Chorus waves are naturally occurring electromagnetic waves in the Earth's magnetized space known as the magnetosphere, and they typically have two frequency bands. A previous study proposed that the banded characteristics is produced by two anisotropic electron populations.

This study aims to address two basic questions about banded chorus waves: 1) are chorus frequency gaps formed near the equatorial source region or during propagation away from equator? and 2) why are chorus frequency gaps usually located below 0.5 f_{ce} (f_{ce}: electron gyro-frequency)? Van Allen Probe spacecraft data reveals that chorus frequency gaps are formed in the equatorial source region where the waves propagate both in the parallel and anti-parallel directions to the magnetic field. By showing the electron distribution in association with banded chorus waves, we explain that initially generated chorus waves quickly accelerate electrons as they propagate away from equator, and the electrons being accelerated at high latitudes lead to a chorus gap below 0.5 f_{ce} when they bounce back to the equatorial source region.

1. Introduction

Whistler-mode chorus waves in the Earth's magnetosphere typically have two frequency bands (*Tsurutani and Smith*, 1974; *Santolík et al*., 2003), namely, the upper band and the lower band, separated by a spectral gap located around half of the equatorial electron gyro-frequency (0.5 f_{ce}). Chorus waves play a critical role in accelerating electrons to MeV energies (*Horne et al*., 2005*; Reeves et al.*, 2013; *Thorne et al*., 2013) and scattering ~0.1-100 keV electrons, precipitating them to the atmosphere to form diffuse and pulsating aurorae (*Thorne et al.*, 2010; *Nishimura et al.*, 2010).

Chorus waves are generated by anisotropic electrons with higher perpendicular temperature than parallel temperature ($T_{\perp} > T_{\parallel}$) through cyclotron resonance (*Kennel*, 1966). Numerous mechanisms have been proposed to explain the banded structure, and the core question that has been under debate is whether chorus waves around 0.5 f_{ce} are not generated in the source or are gradually damped as chorus waves propagate to higher latitudes. Many explanations suggest that chorus gaps are formed as the waves propagate away from the equator (e.g., *Tsurutani and Smith*, 1974; *Omura et al*., 2009; 2020; *Bortnik et al*., 2006). Recent statistical studies (*Gao et al*., 2019; *Teng et al*., 2019) show that banded chorus waves are mostly observed within ~6° in magnetic latitude (MLAT), which favors that chorus gaps are formed in the equatorial source region. However, recent studies (*Hsieh and Omura*, 2018; *Omura*, 2020; *Chen et al*., 2021) suggested that the chorus waves around 0.5 fce can be significantly damped during propagation at only a few degrees away from equator.

A competing mechanism proposed that chorus gaps are formed in the source region. *Liu et al*., (2011) and *Fu et al*. (2014) suggested the banded chorus waves may be generated at the source region from two distinct anisotropic electron populations at different energies. *Li et al*. (2019) showed that in association with banded chorus waves, an ubiquitous plateau in the electron phase space density (PSD) occurs at around half of the electron Alfven velocity (0.5 v_{Ae}) and separates two anisotropic electron populations. They revealed that initially generated chorus waves can quickly isotropize the electrons at Landau resonant energies, leading to the separation of the anisotropic electrons into two components. Self-consistent particle-in-cell (PIC) experiments (*Ratcliffe and Watt*, 2017; *Li et al*., 2019; *Chen et al*., 2021) successfully reproduced the electron PSD plateau and the chorus gap around 0.5 f_{ce}, supporting this idea. To determine where the gaps

are actually formed and thus to tackle the generation mechanism of banded chorus waves, the core approach is to accurately identify the source region and survey chorus wave spectra therein.

An important feature of the chorus spectral gap that has been shown in past studies is that the gaps are not symmetric about, but generally occur below the equatorial 0.5 f_{ce}, and the upper-band usually arises from a frequency very close to 0.5 f_{ce}. The statistical distribution of chorus gap frequency shows a center at 0.45 - 0.5 f_{ce} (*Gao et al.*, 2019). In addition, banded chorus waves in the Jovian (*Coroniti et al.*, 1980; *Scarf et al.*, 1981; *Kurth et al.*, 2001) and Saturnian magnetospheres (*Hospodarsky et al.*, 2008; *Menietti et al.*, 2008) show similar spectral gaps below 0.5 f_{ce}. The question of why chorus spectral gaps are usually located below 0.5 f_{ce} has not been fully explained and is the topic of the present study.

The present study mainly focuses on case studies based on Van Allen Probes observations (*Mauk et al.*, 2013). The waves and the DC magnetic fields are provided by the Electric and Magnetic Field Instrument Suite and Integrated Science suite (*Kletzing et al.*, 2013). Specifically, the waveform receiver (WFR) of the Waves instrument provides the survey-mode electric and magnetic wave in a frequency range of ~10 Hz to 12 kHz and the burst-mode waveforms with a sampling rate of 35 k samples/s. The high-frequency receiver (HFR) provides the electric wave measurements over a frequency range of 10–400 kHz, covering the upper hybrid resonance frequency from which the plasma density can be inferred (*Kurth et al.*, 2015). The Helium, Oxygen, Proton, and Electron (HOPE) instrument (*Funsten et al.*, 2013; *Spence et al.*, 2013) provides electron distributions over an energy range from 15 eV to 51 keV.

2. Are chorus spectral gaps formed at the source region or during propagation?

Chorus waves have wave vectors predominantly quasi-parallel to the background magnetic field and propagate both northward and southward away from the equator; therefore, the coexistence of parallel and anti-parallel propagating waves can be used to identify the chorus source region. Here we present Van Allen Probe B observations on 8 May 2016. Figure 1a shows the plasma density and the ratio between the electron plasma frequency and the electron gyro-frequency (f_{pe}/f_{ce}), derived from the HFR wave measurements shown in Figure 1b and the magnetometer data. The magnetic and electric wave spectral intensities measured by the WFR, shown in

Figures 1c and 1d respectively, show chorus waves that were almost continuously observed over 6.5 hours. The wave normal angle with respect to the ambient magnetic field, shown in Figure 1e, indicates that chorus waves were mostly quasi-parallel (or quasi-anti-parallel) propagating. The spacecraft was initially in the southern hemisphere and traveled to the northern hemisphere according to the MLAT derived from the TS04 model (*Tsyganenko and Sitnov*, 2005). Figure 1f presents the Poynting flux angle with respect to the ambient magnetic field, showing several reversals between near-parallel and near-antiparallel wave propagation at low latitudes from 07:30 UT to 11:30 UT, suggesting that the spacecraft located near or within the source region. Chorus spectral gaps were almost persistently observed during this period, indicating the existence of chorus gaps in the source region. As the satellite traveled away from the equator to the northern hemisphere after 11:30 UT, the chorus waves were seen to become steadily northward propagating, indicating exit from the source region.

Figure 2a show the burst-mode wave spectra at 08:02 UT. Figure 2b shows the wave normal angle calculated using the *Means* (1972) method. The Poynting flux angle presented in Figure 2c shows that the parallel and anti-parallel propagating waves were interleaved in the lower band, indicating that the spacecraft was traveling through the source region. The upper band chorus also exhibits both parallel and anti-parallel propagating components, while it is dominated by anti-parallel propagating component, possibly because the source region of the upper-band is more spatially compact than that of the lower-band. A survey of the burst-mode data during 07:30-11:00 UT suggests that the majority of banded chorus waves were a mixture of parallel and anti-parallel elements, and we show two additional observations in supporting information Figure S1. These observations reveal that chorus spectral gaps are formed in the source region near the equator. This is consistent with the statistical results that banded chorus waves are mostly observed close to the magnetic equator and within ±6°, while single-band chorus waves are observed over a slightly wider latitude range (*Gao et al*., 2019, *Teng* et al., 2019). The previous hypothesis that chorus spectral gaps are developed during propagation would predict that single-band chorus waves are closer to the equator, contrary to the statistical results.

3. Why are chorus gaps usually observed below 0.5 fce?

The banded chorus waves shown in Figure 2a are a typical case that has a spectral gap occurring predominantly below 0.5 f_{ce} and Figure 3a shows the 2-min averaged electron PSD associated

with these banded chorus waves. The electron PSD distribution shows a plateau starting from 1.17 keV at the low pitch angles. The electron distribution has the smallest anisotropy in the range of 2.7 - 5 keV, which separates two pronounced anisotropic components in the lower (~0.1 – 1 keV) and higher (>5 keV) energies.

Figure 3b shows the resonant velocities and the corresponding minimum resonant energy for Landau ($\omega - k_{\parallel} v_{\parallel} = 0$) and cyclotron ($\omega - k_{\parallel} v_{\parallel} = \omega_{ce}$) resonances under the condition f_{pe}/f_{ce} = 7 (which is taken from Figure 1e). Here, $\omega = 2\pi f$, and $\omega_{ce} = 2\pi f_{ce}$. Color coded are three wave normal angles, 5°, 15° and 30°. The Landau resonant velocity changes slightly as a function of frequency and wave normal angle, and maximizes at 0.5 v_{Ae}. (This applies for conditions f_{pe}/f_{ce} >2, which is usually valid at the equator of the outer radiation belt.) The electron Alfven velocity v_{Ae} is defined as $B/\sqrt{\mu_0 m_e n}$, or equivalently, $c \cdot f_{ce}/f_{pe}$. Here, m_e is the electron mass, n is the electron number density, μ_0 is the vacuum magnetic permeability, and c is the light speed in vacuum. The electron PSD at 18° pitch angle shows a plateau starting from 1.17 keV, which corresponds to $v_{\parallel} = 0.45\, v_{Ae}$, suggesting Landau resonant acceleration at the equator.

The reduced electron anisotropy is observed mainly above 0.5 v_{Ae}, up to an energy of ~ 5.2 keV. Our investigations indicate that banded chorus waves with gaps below 0.5 f_{ce} are highly correlated with two anisotropic electron components and an isotropized population above 0.5 v_{Ae}. Figure S2 in the supporting information shows 9 snapshots of electron distributions observed from 07:30 UT to 11:30 UT, demonstrating that banded chorus waves throughout this event were associated with electron parallel acceleration and reduced anisotropy above 0.5 v_{Ae}.

According to linear wave-particle interaction theory, Landau resonance at the equator can only accelerate electrons to a parallel velocity around 0.5 v_{Ae}, corresponding to 1.45 keV for an 18° pitch angle electron in the current case. The reduced anisotropies observed at energies up to 5.2 keV are probably caused by Landau resonance occurring at higher latitudes. This is because $B \propto \sqrt{1 + 3\sin^2\lambda}\,/\cos^6\lambda$ in the dipole field, and $n \propto 1/\cos^{\alpha}\lambda$ where $\alpha = 1.6 - 4.2$ in an empirical model (*Denton et al.*, 2004; 2006). Thus, the representative Landau resonant velocity $0.5\, v_{Ae} \propto B/\sqrt{n}$ increases with latitude λ rapidly. In the present study, we adopt a median value $\alpha = 2.8$, and the latitudinal variations of B, n and v_{Ae} are shown in Figure 3c. The reduced anisotropy at 5.2 keV in Figure 3a corresponds to 0.5 v_{Ae} at a latitude of ~26°, implying a strong resonant interaction up to that point.

The parallel acceleration and the resultant isotropization above 0.5 v_{Ae} is more pronounced than that below 0.5 v_{Ae}, possibly because the waves propagate away from equator, and the Landau resonant interaction occurs mostly at higher latitudes. In addition, the chorus waves in this case are quasi-parallel in the source region, and the Landau damping rate is weak (note that the Landau damping rate approaches 0 as the wave normal angle approaches 0°). These chorus waves become increasingly oblique as they propagate to high latitudes (e.g., *Bortnik et al*., 2007, 2008), leading to stronger Landau resonant acceleration with increasing latitude. The accelerated electrons are then reflected to the source region by the mirror force, forming a new electron distribution as was observed by the spacecraft. The isotropized population above 0.5 v_{Ae} suppresses the chorus excitation just below 0.5 f_{ce} and thus forms the spectral gap.

We use linear growth theory (*Kennel*, 1966) to demonstrate the formation of the chorus gap due to parallel acceleration. Following previous studies (e.g., *Li et al*., 2017), the observed electron PSD is fitted as a combination of kappa distributions and Gaussian distributions, which are expressed as

$$f = \frac{n_0 2^{2\kappa-1}(\kappa - 1/2)\Gamma^2(\kappa)}{\pi^2\sqrt{\kappa}\Gamma(2\kappa)v_{T\perp}^2 v_{T\parallel}}\left(1 + \frac{v_\perp^2}{\kappa v_{T\perp}^2} + \frac{{v_\parallel}^2}{\kappa v_{T\parallel}^2}\right)^{-\kappa-1},$$

and

$$f = \frac{n_o}{\pi^{3/2}v_{T\perp}^2 v_{T\parallel}}\exp\left(-\frac{v_\perp^2}{v_{T\perp}^2} - \frac{(v_\parallel - v_b)^2}{v_{T\parallel}^2}\right),$$

respectively. Here $(v_\perp, v_\parallel)$ are the particle velocities in the transverse and parallel directions with respect to the background magnetic field, and $(v_{T\perp}, v_{T\parallel})$ the perpendicular and parallel thermal velocities. The beam velocity is represented by v_b, and n_0 is the number density. The κ index is the exponent of the Kappa distribution at high energies, and the expression $\Gamma(\kappa)$ is the Gamma function.

Distribution	Density (cm^{-3})	$v_{T\perp}$ (km/s)	$v_{T\parallel}$ (km/s)	v_b (km/s)
Kappa, κ=2	11	700	700	0
Kappa, κ=3	0.52	5,200	3,000	0

Gaussian	0.01×2	20,000	10,000	$\pm$29,000
Kappa, κ=4	0.22	20,000	9,000	0
Kappa, κ=2	0.25	32,000	24,000	0

Table 1. The fitting parameters for the electron distribution averaged over 08:01-08:03 UT observed by Van Allen probe B.

The linear growth theory requires that the electron anisotropy $A = T_\perp/T_\parallel - 1$ should exceed $f/(f_{ce}\text{-}f)$ to excite chorus waves at frequency f (*Kennel and Petschek*, 1966). We note that the anisotropy of the measured distribution is not large enough to excite chorus waves in the upper-band and the lower-band. Previous statistical surveys show that the electron anisotropy associated with chorus waves is usually below the marginal instability levels (*Yue et al*., 2016; *An et al*., 2017), possibly because the anisotropic distribution had already been relaxed by the time the wave is observed. In addition, nonlinear interaction may play an important role which is still to be understood, and it is possible that the nonlinear marginal instability condition deviates from the linear one. We therefore use larger anisotropies than observed to fit the original electron distribution (before it has been relaxed by the wave excitation process), as has been commonly used in previous studies (e.g., *Fu et al*., 2014; *Li et al*., 2019). The parameters for each component are shown in Table 1. The anisotropy for generating the upper-band is $A = T_\perp/T_\parallel - 1 = 3.9$, and that for the lower-band is 0.78. A beam population (and another beam with the opposite bulk velocity for symmetry) is used to model the parallel acceleration effect.

Figure 4a shows the comparison between the fitted and the observed distributions. The wave linear growth rate is calculated using the fitted distribution, and the total growth rates, shown in Figure 4b, are the total effect due to the 1st-order cyclotron resonance and Landau resonance. The contribution from high-order and negative-order resonances are negligible in this case. The growth rates capture the main feature of the chorus power spectrum in Figure 2, that is, chorus waves are separated into two bands, and the gap is mainly below 0.5 f_{ce}. The exact wave frequency range differs slightly between the observed power spectrum and the growth rates, possibly because the linear growth rate represents the wave growth rate at the initial linear stage, and therefore is not proportional to the wave spectrum which reflects the wave intensity after the

nonlinear saturation phase. Besides, the fitted electron distribution we used for calculating the growth rates differs slightly from the real electron distribution. The fitted electron distribution produces a chorus gap centered below 0.5 f_{ce}, which is the result of the reduced anisotropy above 0.5 v_{Ae}.

Previous PIC simulations used a uniform background magnetic field, and the Landau resonant velocity did not vary along the field line. Consequently, the chorus gaps are more symmetric with respect to 0.5 f_{ce} (*Li et al*., 2019, *Chen et al*., 2021). Chorus waves in the magnetosphere with a spectral gap centered above 0.5 f_{ce} (e.g., *Santolík et al*., 2010) have been reported only rarely. For those cases, it is possible that a PSD plateau is initially created within a high-density region, and then drifts to a nearby low-density region. In these cases, the previously generated PSD plateau becomes significantly below 0.5 v_{Ae} at the new location, leading to a chorus gap above 0.5 f_{ce}.

The discrete, rising-tone chorus elements indicate that a nonlinear interaction takes place during the wave excitation (see *Tao et al., 2021* and references therein). Nevertheless, the linear theory has been successful in revealing the initial stage of wave excitation and explaining many features of whistler-mode waves, e.g., the excitation threshold (e.g., *Kennel and Petschek*, 1966; *Li et al.*, 2008) and the wave normal angles (e.g., *Li et al.*, 2016; *Teng et al*., 2019). The linear growth theory provides a foundational understanding of the formation location and the frequency of chorus spectral gaps, while the discrete rising-tone feature of two chorus bands is still left to be fully understood.

4. Conclusions

This study addresses two important questions about the generation of banded chorus waves by investigating Van Allen Probe observations in the source region. The source region is identified by using the coexistence of parallel and anti-parallel propagating chorus waves. Observations of banded chorus waves that consist of interleaved parallel and anti-parallel elements indicate that chorus gaps are formed in the equatorial source region, instead of being developed advectively as the waves propagate to higher latitudes. By showing electron PSD plateaus around 0.5 v_{Ae} and the reduced anisotropy above 0.5 v_{Ae}, we conclude that chorus gaps below 0.5 f_{ce} are due to electron parallel acceleration above 0.5 v_{Ae} that have already occurred due to Landau resonances at higher latitudes. We suggest that chorus waves generated early in the process accelerate the

electrons' parallel velocity to above 0.5 v_{Ae} when propagating to higher latitude, and meanwhile are gradually damped. Landau resonant acceleration at higher latitudes leads to reduced electron anisotropies at higher energies, and the altered electron distribution, when bounce back to the equator, produces banded chorus waves with a wider gap.

The lower limit of chorus spectral gaps and the energy range of electron isotropization can be used to estimate the latitude range of chorus wave damping via Landau resonance. For instance, the electron distribution measured around 08:01 UT in the present case study suggests that the chorus waves might be significantly damped at latitudes below 26°. This may also explain no-gaps chorus, which preferentially occurs on the dayside (e.g., Teng et al., 2019) where Landau damping of chorus waves is weak. The formation of chorus spectral gap below 0.5 f_{ce} and the concurrent electron redistribution can be applied to studies of planetary magnetospheres.

Acknowledgement

JL, JB and XA acknowledge the NSF grant AGS-1923126, NASA grant LWS-80NSSC20K0201 and 80NSSC21K0522. JL and JB acknowledge the grant DE-SC0010578 and NASA grants 80NSSC18K1227, 80NSSC21K0522 and NNX14AI18G. XA and JB acknowledge the NASA grant 80NSSC20K0917. WL acknowledges the NASA grants 80NSSC20K1506, 80NSSC19K0845, and 80NSSC20K0698, NSF grant AGS-1847818, as well as the Alfred P. Sloan Research Fellowship FG-2018-10936. This work (including support for WK) is supported by RBSP-ECT and EMFISIS funding provided by JHU/APL contract No. 967399 and 921647 under NASA's prime contract No. NAS5-01072.

Open Research

The Van Allen Probe data analysis is carried out using the publicly available SPEDAS software (http://spedas.org). The Van Allen Probe data are publicly available from https://rbsp-ect.newmexicoconsortium.org/data_pub/ and https://emfisis.physics.uiowa.edu/Flight/.

References

An, X., C. Yue, J. Bortnik, V. Decyk, W. Li, and R. M. Thorne (2017), On the parameter dependence of the whistler anisotropy instability, J. Geophys. Res. Space Physics, 122, 2001–2009, doi:10.1002/2017JA023895.

Bortnik, J., U. S. Inan, and T. F. Bell (2006), Landau damping and resultant unidirectional propagation of chorus waves, Geophys. Res. Lett., 33, L03102, doi:10.1029/2005GL024553

Bortnik, J., R. M. Thorne, and N. P. Meredith (2007), Modeling the propagation characteristics of chorus using CRRES suprathermal electron fluxes, J. Geophys. Res., 112, A08204, doi:10.1029/2006JA012237.

Bortnik, J., Thorne, R. M., & Meredith, N. P. (2008). The unexpected origin of plasmaspheric hiss from discrete chorus emissions. Nature, 452(7183), 62–66. https://doi.org/10.1038/nature06741

Chen, H., Gao, X., Lu, Q., Sauer, K., Chen, R., Yao, J., & Wang, S. (2021). Gap formation around 0.5Ωe of whistler-mode waves excited by electron temperature anisotropy. Journal of Geophysical Research: Space Physics, 126, e2020JA028631. https://doi.org/10.1029/2020JA028631

Coroniti, F. V., Scarf, F. L., Kennel, C. F., Kurth, W. S. and Gurnett, D. A. (1980), Detection of Jovian whistler mode chorus; Implications for the Io torus aurora. Geophys. Res. Lett., 7: 45-48. doi:10.1029/GL007i001p00045

Denton, R. E., Menietti, J. D., Goldstein, J., Young, S. L. & Anderson, R. R. (2004), Electron density in the magnetosphere. J. Geophys. Res. 109, A09215.

Denton, R. E., K. Takahashi, I. A. Galkin, P. A. Nsumei, X. Huang, B. W. Reinisch, R. R. Anderson, M. K. Sleeper, and W. J. Hughes (2006), Distribution of density along magnetospheric field lines, J. Geophys. Res., 111, A04213, doi:10.1029/2005JA011414.

Fu, X., et al. (2014), Whistler anisotropy instabilities as the source of banded chorus: Van Allen Probes observations and particle-in-cell simulations, J. Geophys. Res. Space Physics, 119, 8288–8298, doi:10.1002/2014JA020364.

Funsten, H. O. et al (2013). Helium, oxygen, proton, and electron (HOPE) mass spectrometer for the Radiation Belt Storm Probes mission. Space Sci. Rev. 179, 423-484.

Gao, X., Chen, L., Li, W., Lu, Q., & Wang, S. (2019). Statistical results of the power gap between lower-band and upper-band chorus waves. Geophysical Research Letters, 46, 4098–4105. https://doi.org/10.1029/2019GL082140

Horne, R. B., Thorne, R. M., Shprits, Y. Y., Meredith, N. P., Glauert, S. A., Smith, A. J., Kanekal, S. G., Baker, D. N., Engebretson, M. J., Posch, J. L., Spasojevic, M., Inan, U. S., Pickett, J. S., Decreau, P. M., Wave acceleration of electrons in the Van Allen radiation belts. Nature 437, 227–230 (2005). doi:10.1038/nature03939

Hospodarsky, G. B., T. F. Averkamp, W. S. Kurth, D. A. Gurnett, J. D. Menietti, O. Santolik, and M. K. Dougherty (2008), Observations of chorus at Saturn using the Cassini Radio and Plasma Wave Science instrument, J. Geophys. Res., 113, A12206, doi:10.1029/2008JA013237.

Kletzing, C., Kurth, W. S., Acuna, M., MacDowall, R. J., Torbert, R. B., Averkamp, T., … Tyler, J. (2013). The electric and magnetic field instrument suite and integrated science (EMFISIS) on RBSP. Space Science Reviews, 179(1-4), 127–181. https://doi.org/10.1007/s11214-013-9993-6.

Kennel, C. (1966), Low-frequency whistler mode, Physics of Fluids 9, 2190, http://dx.doi.org/10.1063/1.1761588.

Kennel, C. F., and H. E. Petschek (1966), Limit on stable trapped particle fluxes, J. Geophys. Res., 71, 1–28, doi:10.1029/JZ071i001p00001.

Kurth, W. S., D. A. Gurnett, A. M. Persoon, A. Roux, S. J. Bolton and C. J Alexander (2001), The plasma wave environment of Europa, Planetary and Space Science, 49, 345-363, https://doi.org/10.1016/S0032-0633(00)00156-2.

Kurth, W. S., De Pascuale, S., Faden, J. B., Kletzing, C. A., Hospodarsky, G. B., Thaller, S. and Wygant, J. R. (2015), Electron densities inferred from plasma wave spectra obtained by the Waves instrument on Van Allen Probes. J. Geophys. Res. Space Physics, 120: 904– 914. doi: 10.1002/2014JA020857.

Li, W., R. M. Thorne, N. P. Meredith, R. B. Horne, J. Bortnik, Y. Y. Shprits, and B. Ni (2008), Evaluation of whistler mode chorus amplification during an injection event observed on CRRES, J. Geophys. Res., 113, A09210, doi:10.1029/2008JA013129.

Li, W., Mourenas, D., Artemyev, A. V., Bortnik, J., Thorne, R. M., Kletzing, C. A., & Spence, H. E. (2016). Unraveling the excitation mechanisms of highly oblique lower band chorus waves. Geophysical Research Letters, 43, 8867–8875. https://doi.org/10.1002/2016GL070386

Li, J., Bortnik, J., An, X., Li, W., Thorne, R. M., Zhou, M., … Spence, H. E. (2017). Chorus wave modulation of Langmuir waves in the radiation belts. Geophysical Research Letters, 44, 11,713–11,721. https://doi.org/10.1002/2017GL075877

Li, J., Bortnik, J., An, X., Li, W., Angelopoulos, V., Thorne, R. M., et al. (2019). Origin of two-band chorus in the radiation belt of Earth. Nature Communications, 10(1), 4672. https://doi.org/10.1038/s41467-019-12561-3

Liu, K., S. P. Gary, and D. Winske (2011), Excitation of banded whistler waves in the magnetosphere, Geophys. Res. Lett., 38, L14108, doi:10.1029/2011GL048375.

Mauk, B. H., Fox, N. J., Kanekal, S. G., Kessel, R. L., Sibeck, D. G., & Ukhorskiy, A. (2013). Science objectives and rationale for the Radiation BeltStorm Probes mission. Space Science Reviews, 179(1-4), 3–27. https://doi.org/10.1007/s11214-012-9908-y.

Means, J. D. (1972). Use of the three-dimensional covariance matrix in analyzing the polarization properties of plane waves. Journal of Geophysical Research, 77, 5551–5559. https://doi.org/10.1029/JA077i028p05551

Menietti, J. D., O. Santolik, A. M. Rymer, G. B. Hospodarsky, A. M. Persoon, D. A. Gurnett, A. J Coates, and D. T. Young (2008), Analysis of plasma waves observed within local plasma injections seen in Saturn's magnetosphere, J. Geophys. Res., 113,A05213, doi:10.1029/2007JA012856.

Nishimura, Y., Bortnik, J., Li, W., Thorne, R. M., Lyons, L. R., Angelopoulos, V., et al. (2010). Identifying the driver of pulsating aurora. Science,330(6000), 81–84. https://doi.org/10.1126/science.1193186.

Omura, Y., M. Hikishima, Y. Katoh, D. Summers, and S. Yagitani (2009), Nonlinear mechanisms of lower-band and upper-band VLF chorus emissions in the magnetosphere, J. Geophys. Res., 114, A07217, doi:10.1029/2009JA014206.

Omura, Y., Hsieh, Y. (2020), Generation of lower band and upper band whistler-mode chorus emissions and associated electron acceleration in the inner magnetosphere, EGU General Assembly 2020, https://doi.org/10.5194/egusphere-egu2020-2143

Ratcliffe, H. and C. E. J. Watt (2017), Self-consistent formation of a 0.5 cyclotron frequency gap in magnetospheric whistler mode waves, J. Geophys. Res. Space Physics, 122, 8166–8180, doi:10.1002/2017JA024399.

Reeves G. D. et al. (2013), Electron acceleration in the heart of the Van Allen radiation belts. Science 341, 991-994, DOI: 10.1126/science.1237743.

Scarf, F. L., D. A. Gurnett and W. S. Kurth (1981), Measurements of plasma wave spectra in Jupiter's magnetosphere, J. Geophys. Res, 86(A10), 8181-8198, doi: 10.1029/JA086iA10p08181.

Santolík, O., D. A. Gurnett, J. S. Pickett, M. Parrot, and N. Cornilleau-Wehrlin (2003), Spatio temporal structure of storm-time chorus, *J. Geophys. Res.,* 108(A7), 1278, doi:10.1029/2002JA009791

Santolík, O., et al. (2010), Wave-particle interactions in the equatorial source region of whistler-mode emissions, J. Geophys. Res., 115, A00F16, doi:10.1029/2009JA015218.

Spence, H. E., G. D. Reeves, D. N. Baker, J. B Blake, M. Bolton, S. Bourdarie, A. H. Chan, S. G. Claudepierre, J. H. Clemmons, J. P. Cravens, S. R. Elkington, J. F. Fennell, R. H. W. Friedel, H. O. Funsten, J. Goldstein, J. C. Green, A. Guthrie, M. G. Henderson, R. B. Horne, M. K. Hudson, J.-M. Jahn, V. K. Jordanova, S. G. Kanekal, B. W. Klatt, B. A. Larsen, X. Li, E. A. MacDonald, I. R. Mann, J. Niehof, T. P. O'Brien, T. G. Onsager, D. Salvaggio, R. M. Skoug, S. S. Smith, L. L. Suther, M. F. Thomsen, and R. M. Thorne (2013), Science Goals and Overview of the Energetic Particle, Composition, and Thermal Plasma (ECT) Suite on NASA's Radiation Belt Storm Probes (RBSP) Mission, Space Sci. Rev., DOI: 10.1007/s11214-013-0007-5.

393 Tao, X., Zonca, F., & Chen, L. (2021). A "Trap-Release-Amplify" model of chorus waves.
394 Journal of Geophysical Research: Space Physics, 126, e2021JA029585.
395 https://doi.org/10.1029/2021JA029585

396 Teng, Tao, X., & Li, W. (2019). Typical characteristics of whistler mode waves categorized by
397 their spectral properties using Van Allen Probes observations. Geophysical Research Letters, 46,
398 3607– 3614. https://doi.org/10.1029/2019GL082161

399 Thorne, R. M. et al. (2013), Rapid local acceleration of relativistic radiation-belt electrons by
400 magnetospheric chorus. *Nature*, **504**, 411-414, doi: 10.1038/nature12889.

401 Thorne, R. M., Ni, B., Tao, X., Horne, R. B., & Meredith, N. P. (2010). Scattering by chorus
402 waves as the dominant cause of diffuse auroral precipitation. Nature, 467(7318), 943–946.
403 https://doi.org/10.1038/nature09467

404 Tsurutani, B. T., and E. J. Smith (1974), Postmidnight chorus: A substorm phenomenon, J.
405 Geophys. Res., 79(1), 118–127, doi:10.1029/JA079i001p00118.

406 Tsyganenko, N. A., and Sitnov, M. I. (2005), Modeling the dynamics of the inner magnetosphere
407 during strong geomagnetic storms, J. Geophys. Res., 110, A03208, doi:10.1029/2004JA010798.

408 Yue, C., X. An, J. Bortnik, Q. Ma, W. Li, R. M. Thorne, G. D. Reeves, M. Gkioulidou, D. G.
409 Mitchell, and C. A. Kletzing (2016), The relationship between the macroscopic state of electrons
410 and the properties of chorus waves observed by the Van Allen Probes, Geophys. Res. Lett., 43,
411 7804–7812, doi:10.1002/2016GL070084.

Figure Captions

Figure 1. Overview of the wave and plasma measurements by Van Allen Probe B during 07:00-13:30 UT on 08 May 2016. (a) The f_{pe}/f_{ce} ratio and the plasma density provided by the HFR instrument. (b) The electric spectral intensity over 10-500 kHz measured by the HFR instrument. (c) The electric spectral intensity over 0.5-10 kHz measured by the WFR instrument. (d) The magnetic spectral intensity. (e) The wave normal angle between the wave k-vector and the background magnetic field. (f) The Poynting flux angle with respect to the background magnetic field. (g) Energy spectrogram of the omni directional electron flux.

Figure 2. The burst-mode chorus wave measurements at 08:02 UT. (a) Wave magnetic spectral intensity. (b) Wave normal angle; (c) Poynting flux angle.

Figure 3. Electron PSD distribution and resonant velocity. (a) The electron PSD distribution averaged over 08:01-08:03 UT. (b) The minimum resonant energies (resonant velocities) versus wave frequency for Landau (solid lines) and cyclotron resonant interactions (dash-dotted lines). Color coded are different wave normal angles. (c) The latitudinal variation of the dipole magnetic field strength, the plasma density from Denton's empirical model, and the resultant electron Alfven velocity.

Figure 4. Linear growth calculation of wave growth and frequency gap. (a) The color-coded lines (dots) represent the fitted (measured) electron PSD distribution at different pitch angles. (b) The linear wave growth rates at three different wave normal angles calculated for the fitted electron distribution.

Figure 1.

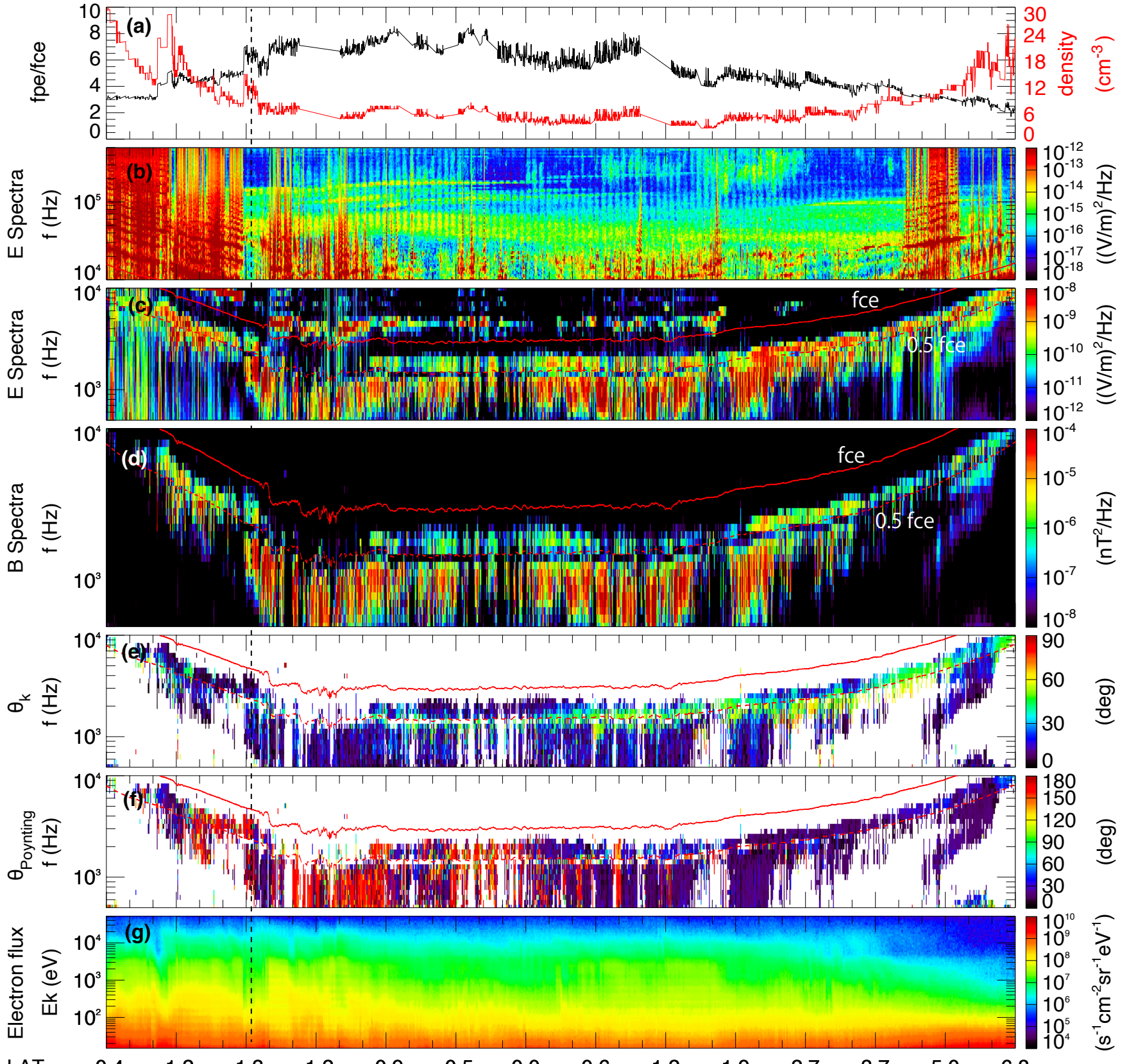
2016-05-08 Van Allen Probe B
(a)
fpe/fce
density (cm-3)
(b)
E Spectra
f (Hz)
((V/m)2/Hz)
(c)
fce
0.5 fce
(d)
B Spectra
(nT2/Hz)
(e)
θk
(deg)
(f)
θPoynting
(g)
Electron flux
Ek (eV)
(s-1cm-2sr-1eV-1)
LAT -0.4 -1.2 -1.3 -1.2 -0.9 -0.5 0.0 0.6 1.2 1.9 2.7 3.7 5.0 6.8
MLT 3.2 4.0 4.6 5.1 5.5 5.9 6.2 6.5 6.9 7.2 7.6 8.1 8.7 9.5
L 3.4 4.1 4.7 5.2 5.5 5.7 5.8 5.8 5.7 5.5 5.2 4.8 4.3 3.6
hhmm 0700 0730 0800 0830 0900 0930 1000 1030 1100 1130 1200 1230 1300 1330
2016 May 08

Figure 2.

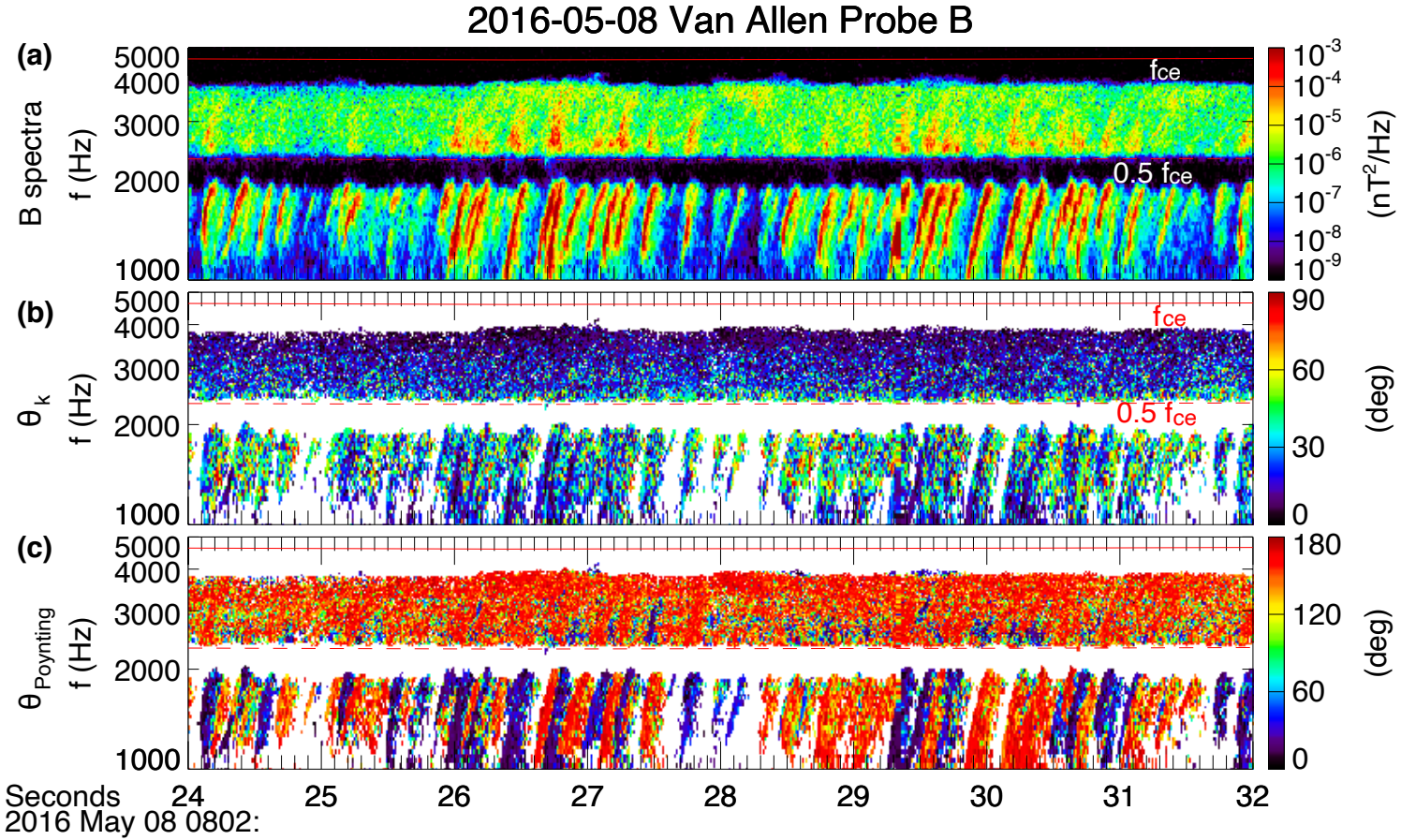
2016-05-08 Van Allen Probe B
(a)
B spectra
f (Hz)
5000
4000
3000
2000
1000
fce
0.5 fce
10^-3
10^-4
10^-5
10^-6
10^-7
10^-8
10^-9
(nT^2/Hz)
(b)
θ_k
f (Hz)
fce
0.5 fce
90
60
30
0
(deg)
(c)
θ_Poynting
f (Hz)
180
120
60
0
(deg)
Seconds
24
25
26
27
28
29
30
31
32
2016 May 08 0802:

Figure 3.

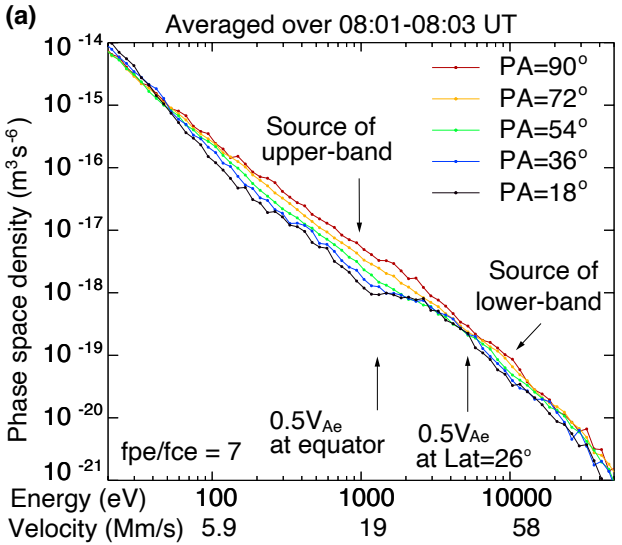
(a)
Averaged over 08:01-08:03 UT
PA=90°
PA=72°
PA=54°
PA=36°
PA=18°
Source of upper-band
Source of lower-band
0.5VAe at equator
0.5VAe at Lat=26°
fpe/fce = 7
Phase space density (m3s-6)
Energy (eV) 100 1000 10000
Velocity (Mm/s) 5.9 19 58

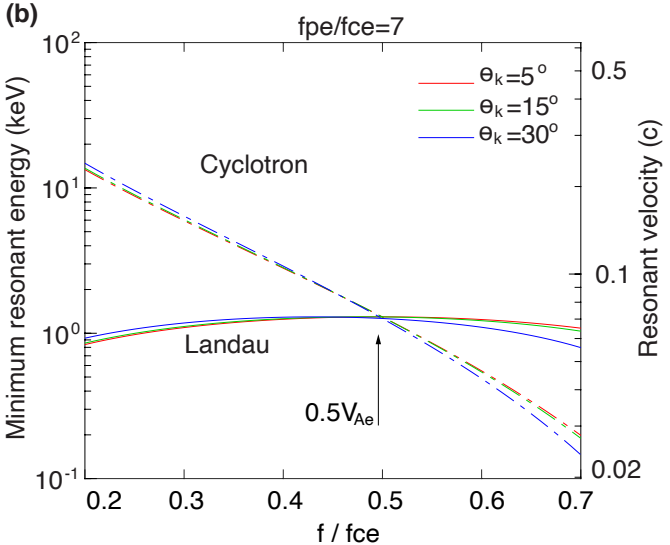
(b)
fpe/fce=7
θk=5°
θk=15°
θk=30°
Cyclotron
Landau
0.5VAe
Minimum resonant energy (keV)
Resonant velocity (c)
f / fce

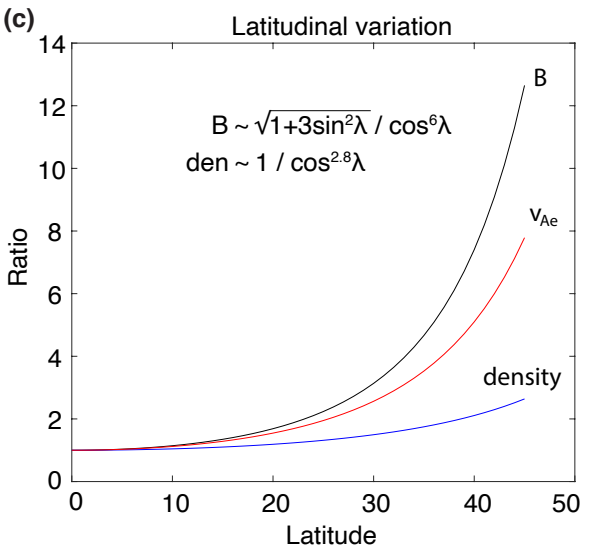
(c)
Latitudinal variation
B ~ √(1+3sin²λ) / cos⁶λ
den ~ 1 / cos^2.8λ
B
VAe
density
Ratio
Latitude

Figure 4.

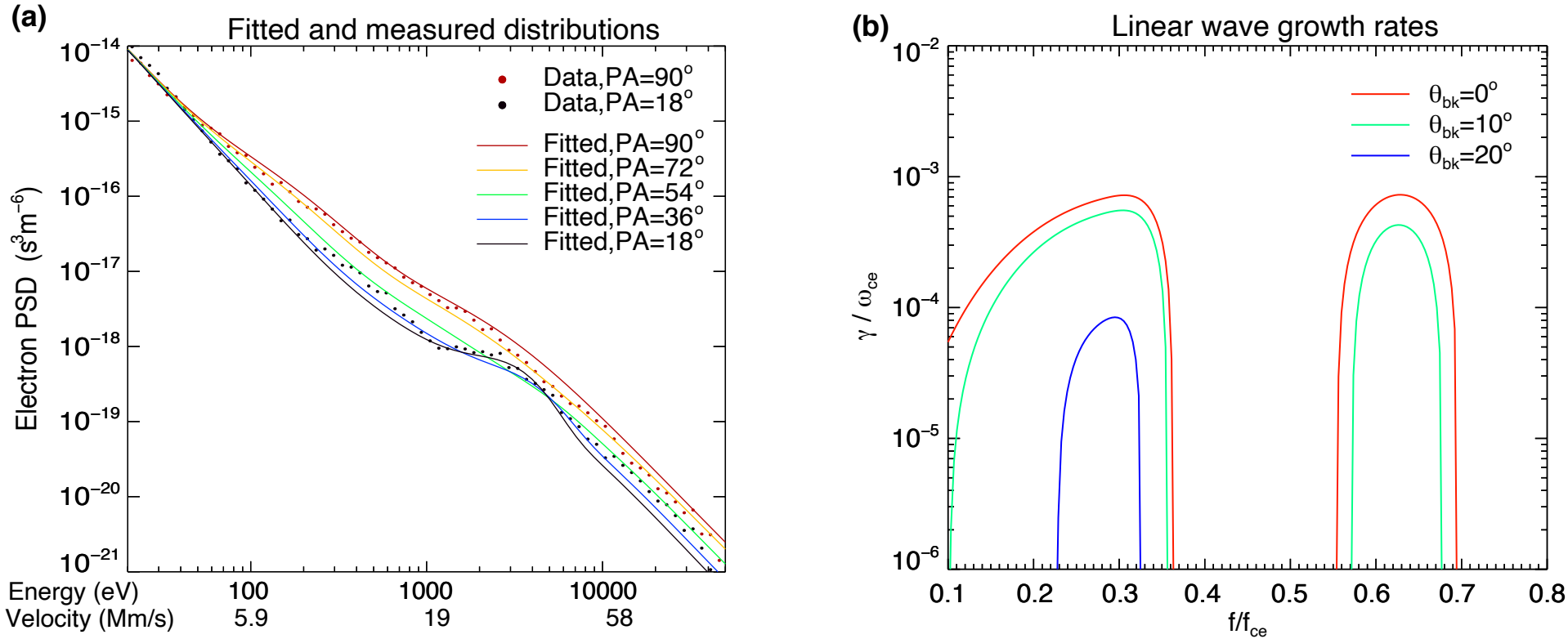
(a)
Fitted and measured distributions
Data,PA=90°
Data,PA=18°
Fitted,PA=90°
Fitted,PA=72°
Fitted,PA=54°
Fitted,PA=36°
Fitted,PA=18°
Electron PSD (s³m⁻⁶)
10⁻¹⁴
10⁻¹⁵
10⁻¹⁶
10⁻¹⁷
10⁻¹⁸
10⁻¹⁹
10⁻²⁰
10⁻²¹
Energy (eV)
Velocity (Mm/s)
100
1000
10000
5.9
19
58
(b)
Linear wave growth rates
θbk=0°
θbk=10°
θbk=20°
γ / ωce
10⁻²
10⁻³
10⁻⁴
10⁻⁵
10⁻⁶
0.1
0.2
0.3
0.4
0.5
0.6
0.7
0.8
f/fce